

Variability and Evolution of African Easterly Wave Structures and Their Relationship with Tropical Cyclogenesis over the Eastern Atlantic

ALAN BRAMMER AND CHRIS D. THORNCROFT

Department of Atmospheric and Environmental Science, University at Albany, State University of New York, Albany, New York

(Manuscript received 17 March 2015, in final form 17 September 2015)

ABSTRACT

African easterly waves (AEWs) are objectively tracked between West Africa and the tropical Atlantic based on the CFSRv2 data for 1979 to 2012. The characteristics of the troughs of the AEWs at the West African coast are explored and related to whether they favor tropical cyclogenesis over the eastern Atlantic. A logistic regression model was used to determine the optimum combination of predictors that relate AEW characteristics to tropical cyclogenesis. The most skillful model for genesis over the eastern Atlantic consisted of four variables of the AEWs dynamics over the coastal region and the absolute number of days from the peak in the AEW season. Using this diagnostic an equal number of favorable developing and nondeveloping waves were compared through a composite difference analysis. Favorable developing waves had significantly higher moisture content in the lower troposphere to the northwest of the trough as they exited the West African coast compared to favorable nondeveloping waves. Trajectory analysis for all the waves revealed that as the AEWs transition over the West African coast the troughs are typically open to the environment ahead and to the northwest of the trough. For developing waves this means that moist air is ingested into the lower levels of the system, while for nondeveloping waves dry air is ingested. At this point in the AEW life cycle this difference may be fundamental in determining whether a favorable wave can develop or not.

1. Introduction

The relationship between tropical cyclogenesis over the Atlantic main development region (MDR) and African easterly waves (AEWs) originating from Africa, has been well documented (e.g., [Reed et al. 1977](#); [Landsea 1993](#); [Thorncroft and Hodges 2001](#)). Many papers have focused on the mean structure and evolution of these African easterly waves (AEWs), documenting their relationship to the African easterly jet (AEJ) and convection over Africa (e.g., [Kiladis et al. 2006](#)). Recently, more attention has been given to studying differences between the developing and nondeveloping waves and why only a small fraction of waves are associated with cyclogenesis in the MDR (e.g., [Hopsch et al. 2010](#); [Agudelo et al. 2011](#)). It was noted by [Hopsch et al. \(2010\)](#) that many AEWs appear to have characteristics that are favorable for tropical

cyclogenesis but do not develop. This paper will highlight in more detail the variability of the waves and the reasons why such favorable waves do not develop.

The large-scale environmental constraints for tropical cyclogenesis have been extensively documented with basic thresholds of certain variables understood to be necessary for genesis. The key characteristics are usually warm sea surface temperatures (SSTs; $>26.5^{\circ}\text{C}$), low magnitude of deep layer vertical wind shear, and moist midlevels ([Gray 1968](#)). Over the eastern Atlantic the large-scale environment restricts genesis to mid-July through early October. Outside of these months either SSTs are generally too cold (June) or shear increases to unfavorable magnitudes (October) (e.g., [Thorncroft and Pytharoulis 2001](#)). During the peak summer months [June–September (JAS)] [Agudelo et al. \(2011\)](#) showed that most of the variance in genesis events over the eastern Atlantic was explained by wave-scale variability rather than long-term environmental factors.

The eastern Atlantic also has the potential negative impacts of the dry Saharan air layer (SAL) outbreaks north of the AEJ. Typically about 28 outbreaks occur during July through September each year ([Laken et al.](#)

Corresponding author address: Alan Brammer, University at Albany, State University of New York, 1400 Washington Ave., Albany, NY 12222.
E-mail: abrammer@albany.edu

2014). The impact of dry air on pregenesis systems is still not conclusive though. Entrainment of dry air into an incipient disturbance may favor convectively driven downdrafts of low entropy air, thus reducing the convective available potential energy at low levels in the disturbance (e.g., Emanuel 1989; Dunion and Velden 2004). Observational studies have shown a significant correlation between the presence of dry air in the northwest quadrant and weakening tropical cyclone intensities (Shu and Wu 2009). Fritz and Wang (2013), however, showed that while dry trajectories were able to penetrate near the vortex center of developing systems, transient dry air was moistened while being wrapped in and thus did not impact the deep convection. However, for systems embedded in a more persistently dry environment, upward moisture transport was reduced due to midlevel drying and enhanced by a lack of moisture supply from the boundary layer (Fritz and Wang 2013). Idealized numerical simulations have shown that midlevel dry air has to be within around 150 km of the vortex center for any impact to be felt, though these simulations were in an environment with no mean flow (Braun et al. 2012). When numerical simulations included vertical shear, the tropical systems were more sensitive to the environmental dry air, in better agreement with observational studies (Ge et al. 2013).

Analysis of the troughs with respect to the wave-relative flow is an important concept for understanding the interaction between the disturbances and the surrounding environment. At the jet level there is typically a region of recirculating air in the trough, coined the “pouch” of the wave (Dunkerton et al. 2009). This has been hypothesized to protect the disturbance within this region from the exterior environment and allow the inner region to progressively moisten through convective activity (e.g., Dunkerton et al. 2009; Wang et al. 2010). An important factor in this paradigm is the four-dimensional evolution of the pouch. To benefit from such recirculation, the pouch region should have both temporal and vertical integrity. Changes in the background flow, phase speed, or ascent through the region would potentially negate the benefit of such a recirculation.

Hopsch et al. (2010) presented mean structural differences in trough-scale characteristics as the waves crossed the West African coastline, showing that developing waves were on average characterized by increased low-level vorticity and higher humidity throughout the column in the trough compared to nondeveloping AEWs. Agudelo et al. (2011), in a similar study, found that column-integrated heating, specific humidity, and vertical velocity provided the best statistical predictors of downstream genesis probability. Leppert et al. (2013a,b) observed similar features with

developing waves typically having higher fractional coverage of convective cloud tops below ≤ 240 K over the coastal region. Similar results have also been observed across forecast ensemble members; developing members were more convectively active while crossing the coast compared to the nondeveloping members (Cecelski and Zhang 2013). These results have shown that there are favorable synoptic/mesoscale conditions (e.g., low-level vorticity, increased humidity, convective activity) in AEWs many days prior to cyclogenesis.

The aim of this paper is to present the synoptic-scale differences between waves, focusing on the characteristics of the troughs and the surrounding environment. The variability of a large sample of AEW structures as they leave the West African coast will be presented in section 3. A genesis diagnostic for the waves as they leave the coast will then be presented, which will be used to objectively identify favorable waves. The composite differences between these favorable waves will be presented in section 4 to highlight the key environmental differences influencing genesis over the eastern Atlantic. Forward and backward trajectories will be presented in section 5 to explore the results of section 4 in more detail and investigate the kinematic sources of environmental differences.

2. Methodology

a. Data

This research uses the most recent reanalysis data from the National Centers for Environmental Prediction (NCEP), the Climate Forecast System Reanalysis, version 2 (CFSR v2; Saha et al. 2010). These data span 1979–2012 with a temporal resolution of 6 h and a horizontal resolution of 0.5° . Anomalies are calculated by subtracting a 31-yr (1979–2009) climatology, calculated as the first four harmonics of the mean annual cycle, from every 6-h period rather than daily means so that low-level anomalies were not aliased by the diurnal cycle. NOAA interpolated outgoing longwave radiation (Liebmann and Smith 1996) is also used in this research. This dataset is available at 2.5° resolution once daily over the same time span as the CFSR data used in this study.

b. Significance testing

The statistical significance of composites was tested using a bootstrap method similar to Matthews and Kiladis (1999) and Schreck et al. (2013). This methodology uses the nondeveloping cases as the null cases for comparison with the developing cases. The null hypotheses for the composite analysis were that the developing and nondeveloping waves were comparable.

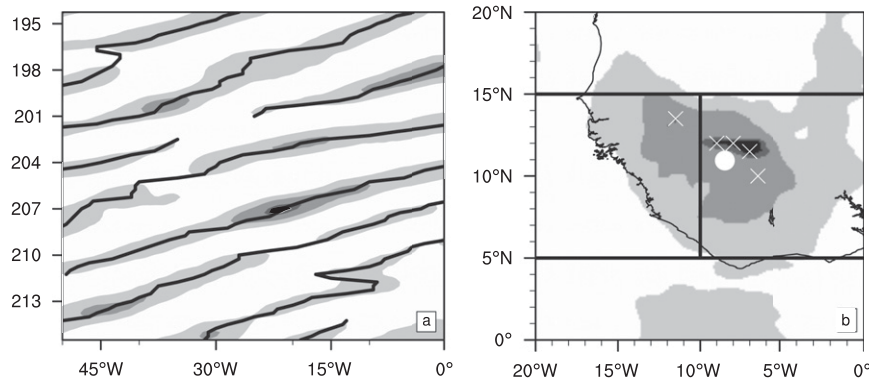


FIG. 1. (a) Hovmöller of curvature vorticity averaged 5°–15°N. Black lines represent initial 2D track of waves on Hovmöller. (b) Example map of unfiltered curvature vorticity (700 hPa), where horizontal lines represent bounds of Hovmöller and the vertical line represents longitude of maxima taken from Hovmöller. White crosses show local maxima and the white dot shows final location of maxima determined through weighted mean of the local maxima.

The test generates 1000 randomly sampled equal-sized composites for both subsets, and significance is found if 975 of the developing composites are either greater than or less than 975 of the nondeveloping composites. This two-tailed test returns significance at the 95% level for each grid cell and is not susceptible to differences in the sample sizes.

c. AEW tracking

As part of this research a tracking methodology was developed that is similar to that used by Agudelo et al. (2011) and Bain et al. (2014) utilizing a Hovmöller to determine the longitudinal track of the waves. AEWs are identified by analyzing radially averaged curvature vorticity (with a radius of 500 km) close to the level of the AEJ (700 hPa). Curvature vorticity at 700 hPa was shown by Berry et al. (2007) to be a useful real-time diagnostic for distinguishing the trough of a wave from the background shear vorticity.

The tracking methodology is done in two steps: 1) a Hovmöller is used to track waves in two dimensions (time and longitude, Fig. 1a), and 2) the tracks are then refined into three dimensions using the Hovmöller “guess” location and the previous latitude or starting at the center of the Hovmöller. Both these steps use the same basic logic, using linear extrapolation of the track over the previous 24 h. Maxima are connected using a cost function combining the expected location and the expected magnitude of the vortex. At times where multiple weak maxima are present, a magnitude-weighted centroid is calculated to select the vorticity centroid at that time (Fig. 1b).

The Hovmöller is used primarily for the waves when they are over Africa where the three-dimensional vortex can be transient in nature. The temporally continuous

synoptic-scale wave is well captured by the Hovmöller whereas a full 3D vortex tracker would define multiple short-lived MCSs or small vortices. When the waves are over the ocean and are less latitudinally restricted, their projection onto the Hovmöller can become separated from the center of the trough if they start to move out of the Hovmöller bounds. At this point, if the track is longer than 4 days and the vortex has been consistently strong, the Hovmöller guess locations are dropped and the tracking relies on the interpolation of the system.

Wave tracks were then matched up with cyclone location data from the Atlantic hurricane database, version 2 (HURDAT2; Landsea et al. 2014). A cyclone was deemed related to the wave if the tropical disturbance was first located within 500 km of the wave maxima. This allows for flexibility in the event of potential errors in both the tracking routine and in the location of disturbances in the reanalysis of dynamic fields (e.g., Schenkel and Hart 2012). Last, waves were only kept if they existed east of 5°W and west of 40°W. Therefore, only well-developed waves that fully transitioned the coastal region of West Africa and into the MDR are retained. For the developing subset here, only tropical cyclogenesis events east of 45°W were included. Systems that developed west of that longitude were excluded from both subsets. This threshold was chosen because of the reduced impact that the characteristics over West Africa will have as the waves move farther from the continent (Hopsch et al. 2010).

The track density of all waves is shown in Fig. 2. The density of tracks is comparable to other tracking papers with maxima over western Africa and the MDR of the Atlantic (e.g., Thorncroft and Hodges 2001; Hodges et al. 2003; Chen et al. 2008). This tracking algorithm is able to detect systems that originate from the Ethiopian

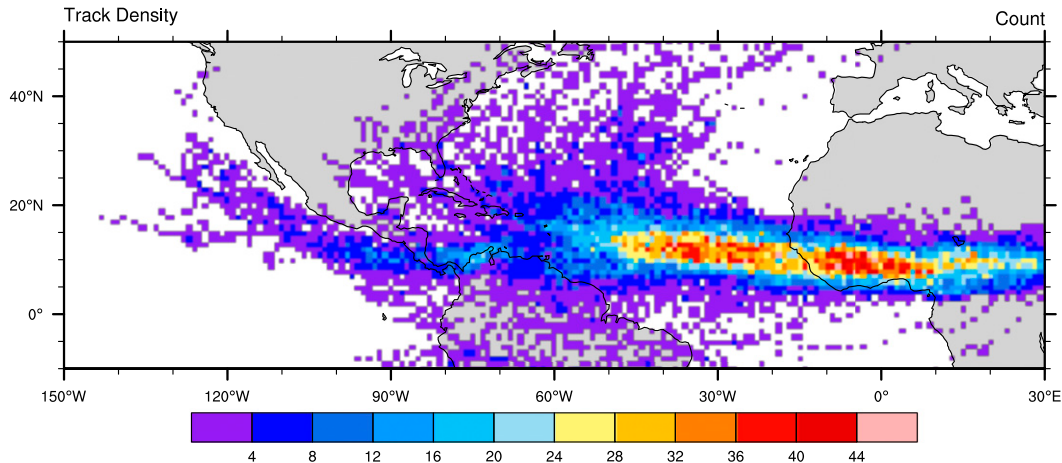


FIG. 2. Count per 0.5° grid of all waves/storms tracked over 1979–2012.

highlands, a potential source of AEW disturbances (Berry and Thorncroft 2005), and waves that transit the whole Atlantic Ocean and cross over to the eastern Pacific. Some of these tracks may develop over the eastern Pacific but were not classified as developing; since only the Atlantic HURDAT data was used to match waves to named systems. This will not impact the results though, as the characteristics of the waves over West Africa and the eastern Atlantic will have very little influence that far downstream.

Waves are composited throughout the paper based on their time relative passage over the coastal region. Members in composites are shifted to the mean location at that time. All composites are, therefore, trough centric with location based on the number of hours from the West African coast. This passage over the coastal region (18°W) will be referred to as day 0 throughout.

d. Logistic regression model

A logistic linear regression model is utilized in section 3 to combine coastal characteristics of the AEWs. The model was developed through the selection and combination of variables, averaged over 500 km around the trough vortex maxima, detailed in section 3. The selection method followed a forward step criteria (Wilks 2011) in which the model was developed iteratively increasing by one variable at a time. Variables were selected at each iterative step based on the lowest mean squared error from the verification set of waves and only coefficients that were significant at $\geq 95\%$ were kept. The forward step development, therefore, had two stopping criteria: either mean squared error did not decrease with additional variables or the additional variables were no longer significant. While it would be possible to develop the model on a large number of

predictors, there is a strong likelihood that the model would then be overfitted and perform poorly outside of the training dataset (e.g., Neumann et al. 1977). Predictors available to the selection process (Table 1) were chosen based on the results presented in section 3 and previous work, as well as variables that have been used in other statistical genesis and intensity models (e.g., DeMaria and Kaplan 1994; Dunion et al. 2013).

The development process trained the models on a random selection of 60% of waves and was tested on the other 40% to avoid overfitting the model to the training set. Once the variables were selected the final model was trained on the whole dataset.

e. Trajectories

Kinematic trajectories were calculated from the 6-hourly 0.5° CFSR data using the HYSPLIT trajectory model (Draxler and Hess 1998). Trajectories were initialized between 10°–20°N and 30°–20°W at 1° horizontal spacing and vertically between 900 and 600 hPa at 50-hPa intervals. These were initialized at the time the trough was closest to 18°W (i.e., over the coast) and run forward for 48 h. Only trajectories initialized more than 350 km from the vortex center were then analyzed. If a trajectory came within 200 km of the vortex center between 12 and 48 h in the forward calculation it was deemed to have been ingested by the trough. While 200 km could be considered large for a mesoscale system, it is less than 10% of the typical AEW wavelength. Backward trajectories were calculated for those forward trajectories that were classified as ingested, with the backward trajectories calculated over the 96 h prior to the wave leaving the coast. Kinematic trajectories from reanalysis data have limitations in their accuracy due to the interpolation methods used. For large-scale flow,

TABLE 1. Predictors used in development of statistical model to diagnose AEW genesis favorability. Boldface variables are those used in the final model, selected via a forward step criteria process.

Climatological and persistence predictors	Synoptic predictors
Absolute value of Julian day 239 (peak day of AEW activity)	850–700-hPa specific humidity
Latitude of system	600-hPa relative humidity
Total phase speed of wave	850-hPa relative vorticity (RV)
<i>U</i> phase speed	850–600-hPa layer average RV
<i>V</i> phase speed	600–850-hPa RV difference
850-hPa RV 5° longitude tendency	800–300-hPa vertical velocity <i>W</i>
	400–200-hPa temperature anomaly
	300–200-hPa divergence
	200-hPa divergence
	200–850-hPa deep vertical shear
	500–850-hPa midtropospheric vertical shear

0.5° and 6-h trajectory calculations have been shown to be reasonably accurate outside of regions of strong ascent (Stohl et al. 1995). Hence, emphasis has been given to the flow prior to ingestion by the system as the convective nature of the disturbance is unlikely to be accurately represented by the reanalysis data.

3. Trough variability

This section will present the evolution and variability of developing and nondeveloping waves, and will highlight characteristics that define waves with the greatest potential to develop over the Atlantic. As reviewed earlier, previous research has highlighted mean differences between developing and nondeveloping waves. The frequency of the characteristics that match developing waves, however, has not been fully explored.

a. Evolution of developing and nondeveloping waves

The evolution of the vertical profile of trough-centric variables is presented in Fig. 3. These profiles show the longitudinal evolution of variables averaged over 500 km around each trough's center. For each wave, variables were averaged azimuthally and radially over 500 km around the trough every 6 h providing an evolution in space and time for each trough. These vertical profiles were then interpolated along a 0.5° longitudinal grid and composited over all troughs. Therefore, each vertical slice represents the profile of the composite trough at that longitude. The hatching on the developing composite shows the regions where there is no significant difference between the developing and nondeveloping composite.

Figures 3a and 3b show the evolution of moisture within the trough of the nondeveloping and developing waves, respectively. Nondeveloping waves are seen to have small positive moisture anomalies around the trough over land. As the waves leave the coast (around 18°W) the mean nondeveloping wave starts to moisten throughout the

lower levels of the trough (700 hPa and below). In comparison, the developing waves have an increased amount of midlevel moisture over West Africa and rapidly moisten throughout the lower troposphere as they approach the coast, passing 20°W with $>0.5 \text{ g kg}^{-1}$ of anomalous moisture between 900 and 400 hPa. As the developing waves leave the coast the entire column (<200 hPa) is significantly moister than the nondeveloping wave composite, with the midlevels (300–800 hPa) being significantly different as far east as 0°.

The evolution of anomalous vertical motion, anomalous temperature, and relative vorticity are also shown in Fig. 3. The developing composites are statistically significantly different from the nondeveloping composite west of around 0°, except temperature, which becomes significantly different between 200 and 300 hPa west of 20°W. Anomalous vertical motion (Figs. 3c,d) shows that nondeveloping waves typically have a convective period over the West African coast, but this is localized to the coastal region. The developing waves show increasing ascent as they approach the coastal region, however the AEW composite then maintains strong ascent over the eastern Atlantic. The thermal anomalies (Figs. 3e,f) associated with the AEW composites show that nondeveloping waves have a small positive temperature anomaly at the mid- to upper levels consistent with convective activity. Developing waves, however, have a much stronger signal throughout the midlevels with a significantly warmer troposphere above 300 hPa from approximately 20°W. As the composite trough progresses westward the significant differences gradually descend through the column. The bimodal peak of temperature in the developing waves is interpreted as increased convective activity in general. The profile is generally consistent with both upper-level heating from stratiform convection and midlevel heating from deep or shallow convection (e.g., Schumacher et al. 2004; Zhang and Hagos 2009; Ling and Zhang 2013).

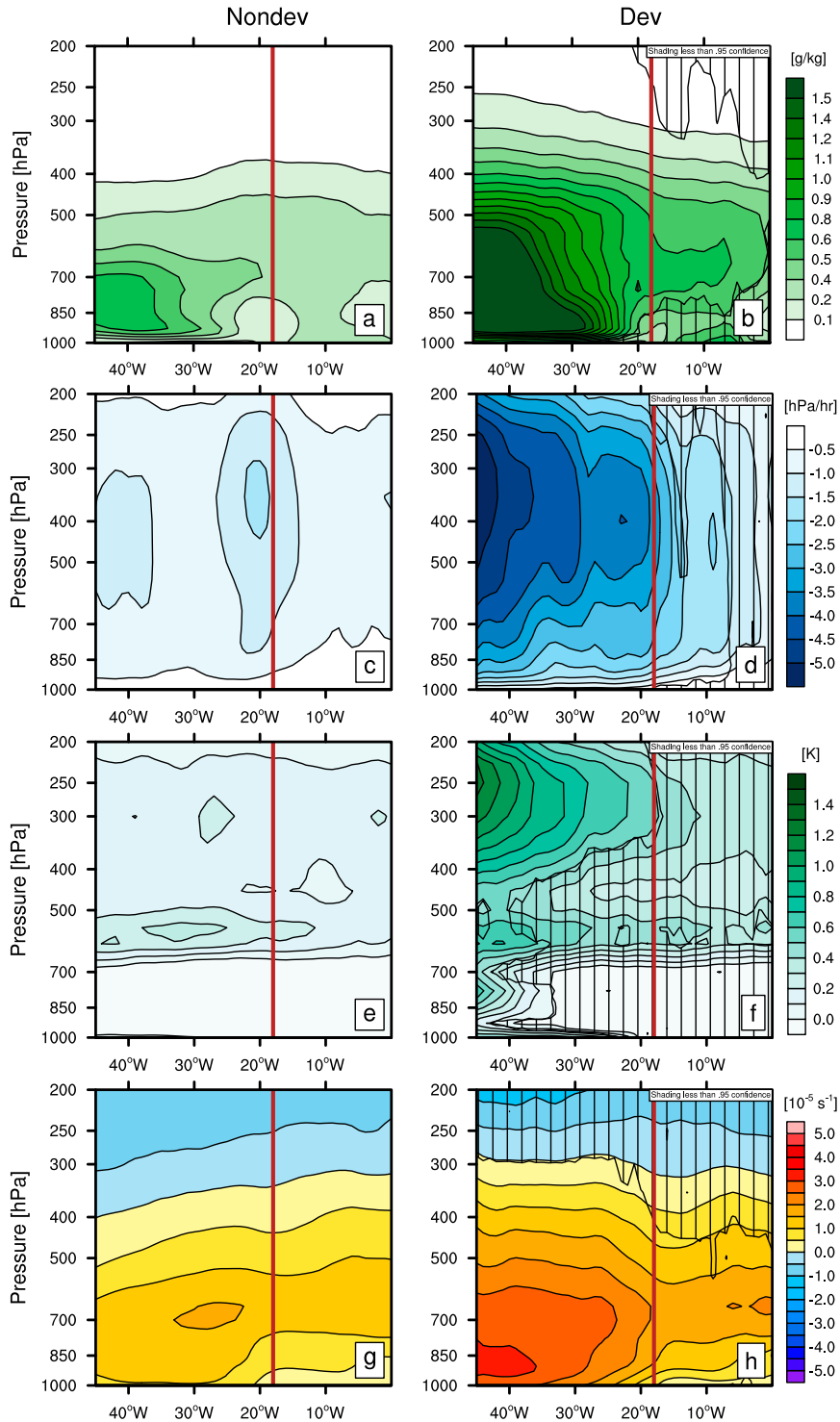


FIG. 3. Vertical evolution of trough centered variables averaged over 500-km radius. (a),(c),(e),(g) Mean nondeveloping waves ($n = 382$) and (b),(d),(f),(h) mean developing waves ($n = 65$). Hatched region denotes areas that are not significantly different to nondeveloping composite at 95%. (a),(b) Anomalous specific humidity (g kg^{-1}). (c),(d) Anomalous vertical motion (hPa h^{-1}). (e),(f). Anomalous temperature (K). (g),(h) Relative vorticity (10^{-5} s^{-1}). Approximate longitude of coast denoted by the vertical brown line.

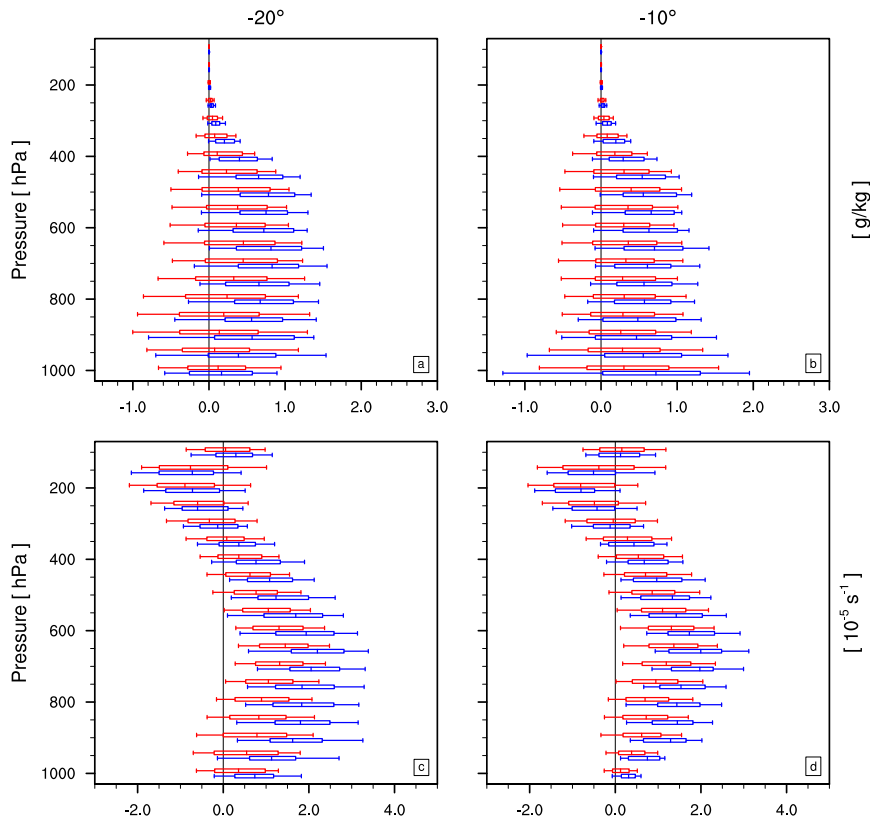


FIG. 4. Distribution of variables with height (y axis) and longitude (columns) of developing (blue) and nondeveloping (red) waves. Ends of whisker represent min/max, box displays the quartile range, and vertical line shows mean. Columns show variability at (a),(c) 20° and (b),(d) 10°W. Rows show (a),(b) specific humidity (g kg^{-1}) and (c),(d) relative vorticity (10^{-5} s^{-1}).

The evolution of trough-based vorticity (Figs. 3g,h) is consistent with the previous figures. Developing waves exhibit a significantly stronger trough throughout the lower troposphere west of 0° , which extends up to 300 hPa upon reaching the coast. As the nondeveloping waves leave the coast a downward extension of the midlevel vorticity is seen between 20° and 30°W . This result is consistent with the mean structures of all AEWs presented by Janiga and Thorncroft (2013) with a downward extension of vorticity occurring when the waves move over ocean. As before, developing waves exhibit stronger vorticity below 400 hPa over land and increase at a faster rate as they approach and leave the coast.

The thermodynamic profiles of the waves are consistent with previous studies concerned with the differences between developing and nondeveloping waves and the evolution of the composite troughs over West Africa and the transition to over the eastern Atlantic (e.g., Hopsch et al. 2010). The composite results here show that in general the mean of all developing waves is distinguishable from the mean of all nondeveloping waves as early as 0° – 5°W across a number of variables

and are already evolving toward a developing system upon reaching the coast. These figures are, however, focused on the composite means and, therefore, conceal the large variability that comprises both composites.

b. Variability in the evolution of developing and nondeveloping waves

This section will present the variability among developing and nondeveloping waves. The overlap in the distributions of the subsets will reveal how frequently the characteristics associated with developing waves occur in the nondeveloping subset. Figure 4 presents the variability of specific humidity and relative vorticity as waves cross 20° and 10°W . These plots highlight the variability contained within the mean structures that were presented in Fig. 3. While the means of both these variables are significantly different at both of these longitude bands, it is clear that there is a large overlap in the distribution of characteristics of both subsets of waves.

At 10°W both the variables show large overlaps in their distributions. Only the top 25% of developing

waves at this point are distinguishable from the non-developing waves (i.e., do not overlap with the non-developing distribution). The largest separations in the characteristic distributions occur at midlevels with around 25% of nondeveloping waves having lower humidity between 500 and 800 hPa than any of the developing waves and, conversely, 25% of the developing waves having higher humidity than any of the non-developing waves. Both sets of waves have a similar moist profile below the jet and a peak in vorticity around the jet level.

At 20°W there is still a large overlap in the distributions of moisture. Above 900 hPa the moisture anomaly has increased across both subsets. However, differences in the relative vorticity distributions become more pronounced as the waves reach the coastal region. Between 50% and 75% of the developing waves have stronger vorticity than 75% of the nondeveloping waves below the AEJ at this location. The vertical extent of vorticity among the developing waves has increased with a maxima between 850 and 600 hPa, while the non-developing waves are still characterized by a pronounced jet-level maximum.

The distributions presented here are a very small example of the overlap in the subsets of these waves. The key point to note here is that, while the means of variables are different, there are potentially a comparable number of nondeveloping waves with characteristics similar to developing waves that are effectively hidden in the large sample size of nondeveloping waves. The trough-scale characteristics presented here can, therefore, be considered as favorable conditions for development but far from sufficient. These results encourage further investigation regarding the differences between nondeveloping and developing waves that have comparable favorable structures and characteristics.

c. Development of an AEW genesis diagnostic

The aim of this section is to define waves that are favorable for development based on a combination of characteristics of the trough prior to leaving the coast. Combining trough-centric variables through a logistic regression model provides a way to objectively define AEWs based on characteristics with respect to downstream cyclogenesis probability. The final iteration of the logistic regression model included five predictors that were all significant within the model at 95% or greater. These variables are shown in the bold text in [Table 1](#).

The resulting combination of variables is physically intuitive and is consistent with the results in the previous section. The coefficients (not presented here) reveal that a combination of increased upper-level temperature anomalies (400–200 hPa), relative vorticity at

850 hPa, ascent throughout the column (800–300 hPa), upper-level divergence (300–200 hPa), as well as the absolute number of days from the peak in the AEW season all point to favorable conditions for development. The first four variables are interpreted to be indicative of convective activity and associated low-level vorticity spinup. Vorticity and anomalous temperature indicate previous convective activity that has modified the trough structure, while ascent and upper-level divergence are representative of current convective activity. These variables do exhibit significant cross correlation between themselves; however, each variable improves the skill of the model significantly. The inclusion of the number days from the peak in the AEW season is a crude metric for capturing the large-scale seasonality in the region.

[Figure 5a](#) shows the frequency of diagnosed genesis probability. The lowest bin of the diagnosed probabilities contains 75% of the nondeveloping waves, which makes clear that the majority of waves leaving the coast do not possess the combined characteristics that would be associated with tropical cyclogenesis. [Figure 5b](#) shows a receiver operator characteristics (ROC) curve for the final logistic regression model. The ROC curve visualizes the rate that the model defines true positives against false positives ([Stanski et al. 1989](#)). A model of random guesses, where the rate of true positives equal false positives, would fall on the $y = x$ dashed line with an area under the curve (AUC) of 0.5; whereas a perfect model would have an AUC of 1.0. The final model used here has an AUC of 0.9, which shows the model has high skill in diagnosing developing and nondeveloping waves. However, this high skill is in a diagnostic sense as the final model was trained on the whole dataset, which for the purposes of this paper is sufficient.

AEWs can, therefore, be objectively defined using a combination of five predictors, which when combined, indicate favorability for genesis within the wave after leaving the coast. The metric will therefore filter out waves that have been defined as unfavorable and thus reduce the obvious differences in the trough-scale features of the waves. A threshold was selected where there were an equal number of developing and nondeveloping waves. This retained 51 favorable developing and nondeveloping waves out of the original sample sizes of 65 and 382, respectively.

The distribution of these favorable waves with respect to day of year and year is shown in [Fig. 6](#). These figures show that there are no obvious interannual differences or seasonal differences between these two subsets of waves. Favorable waves are found to leave the West African coast between late July and late September, with just one early season developing wave in mid-July.

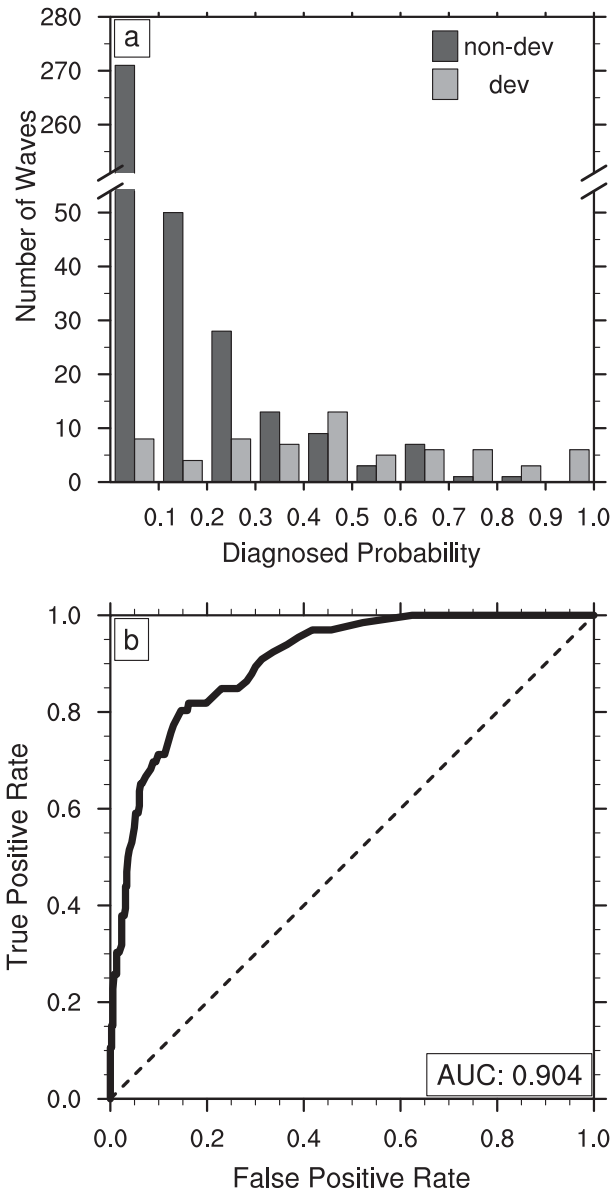


FIG. 5. (a) Frequency of waves binned to 0.1 probability bins. Note the ordinate is broken from 55 to 255. Nondeveloping and developing adjacent bars represent the same bin along the x axis. (b) ROC curve for the AEW genesis diagnostic with the ROC area under the curve included. The dashed line would represent a model of random guesses.

The interannual variability in favorable developing and favorable nondeveloping waves are also similar (Fig. 6b). Also notable in this time series is an increase in the total number of favorable AEWs between 1991 and 2012 that may be related to known influences of the Atlantic multidecadal oscillation (AMO) on AEW characteristics (Martin and Thorncroft 2014). The relative roles played by the AMO and climate change on

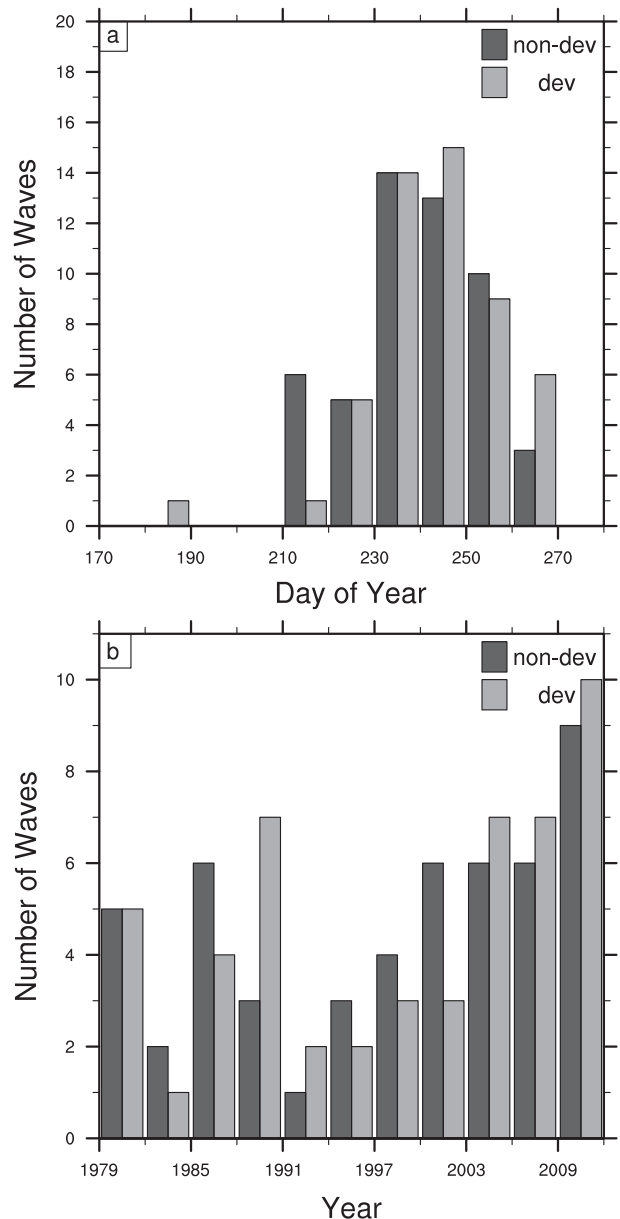


FIG. 6. Frequency of favorable developing and nondeveloping waves. (a) Day of year at 10-day intervals. (b) Year at 3-yr intervals.

favorable AEW structures are interesting topics, but are beyond the scope of this study.

4. Environmental differences in favorable developing and nondeveloping AEWs

The favorable waves defined in the previous section, will now be explored to highlight the extent to which environmental differences can explain the differences between AEWs that develop and those that do not. Because of the selection process, the waves in this

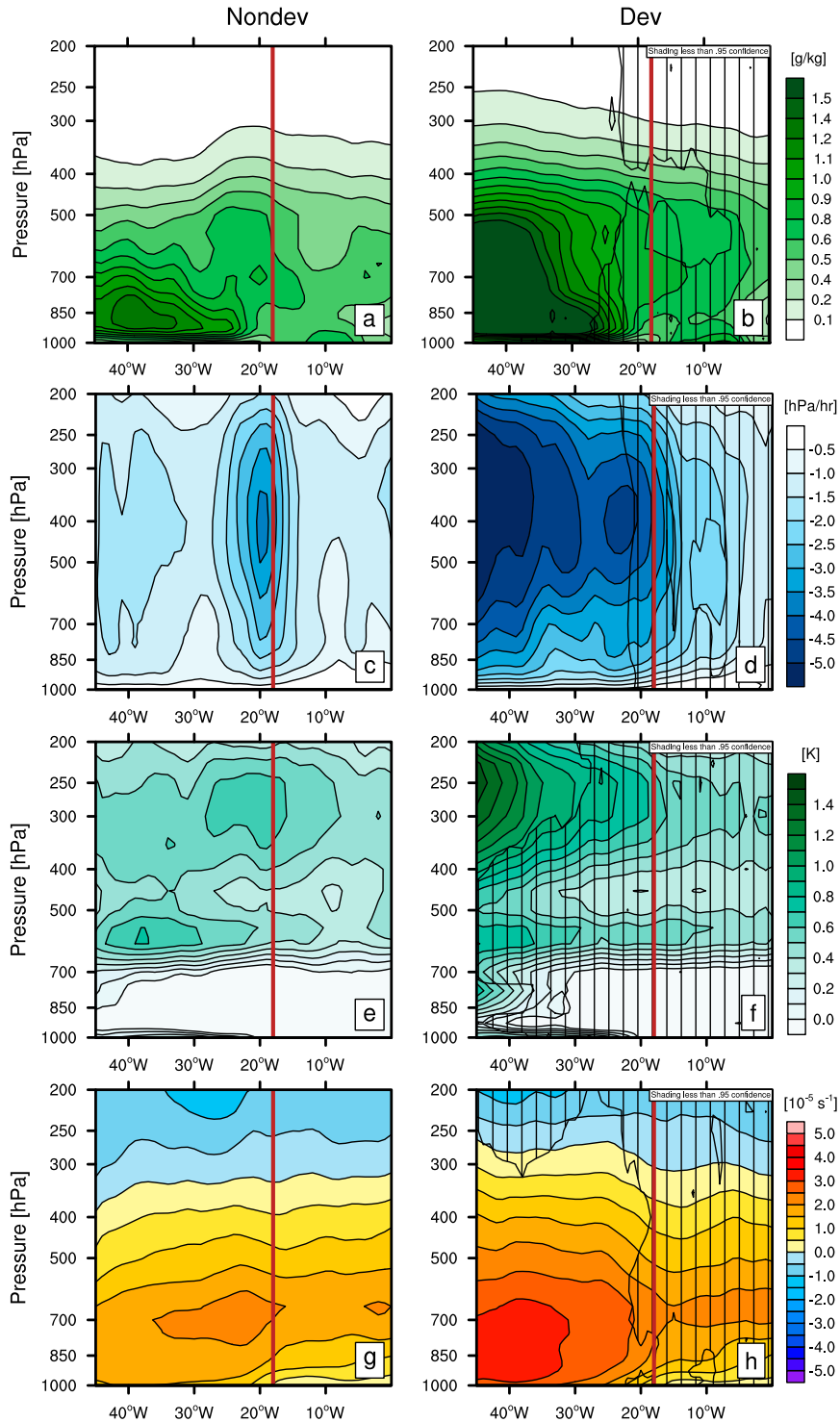


FIG. 7. Vertical evolution of trough centered variables averaged over 500-km radius. (a),(c),(e),(g) Mean favorable nondeveloping waves ($n = 51$) and (b),(d),(f),(h) mean favorable developing waves ($n = 51$). The hatched region denotes the area not significantly different to the nondeveloping composite at 95%. (a),(b) Anomalous specific humidity (g kg^{-1}). (c),(d) Anomalous vertical motion (hPa h^{-1}). (e),(f) Anomalous temperature (K). (g),(h) Relative vorticity (10^{-5} s^{-1}). The approximate longitude of the coast is denoted by the vertical brown line.

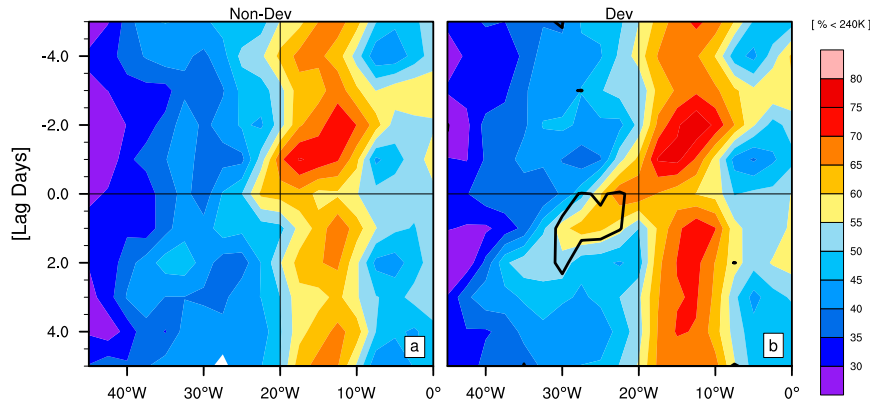


FIG. 8. Mean composite percentage of OLR grid cells ≤ 240 K between 5° and 15° N days -5 to $+5$ of transition over the coastal region for (a) nondeveloping and (b) developing waves. Regions that are significantly different at 95% are outlined by the black contours.

section should be structurally comparable as they leave the West African coast. Therefore, differences between the two subsets should be at distances greater than the 500-km radius used for the variable averages in the previous section.

a. Evolution of favorable AEWs

Figure 7 shows the evolution of the favorable developing and nondeveloping waves. The regions of hatching (nonsignificant differences) now extend west to the coast across the four variables consistent with all the AEWs being favorable for genesis. The differences between these favorable composites, toward the left side of the figure, are expected as the developing waves will possess the characteristics of a tropical depression before 45° W. After leaving the coastal region, the two composites quickly exhibit significant differences in moisture, ascent, and vorticity throughout the column. Nondeveloping waves exhibit strong ascent over the coastal region but rapidly weakens once over the ocean (Fig. 7c). Moisture, vorticity, and temperature all increase in the favorable nondeveloping wave composite more than was shown in the composite of all nondeveloping waves (Fig. 3). Developing waves, however, have continued ascent after leaving the coast and increases in moisture, vorticity, and upper-level temperature are significantly greater.

These figures have shown that the two subsets of waves are not significantly different over West Africa or the coastal region. The significant differences between the favorable subsets are solely in their evolution after leaving the coast.

The differences between the composites after leaving the coast are suggestive of differences in modeled convection and associated latent heat release over the eastern Atlantic. To assess whether there is a significant

difference in observed convection for these two samples, we present an analysis of the fractional coverage of cold cloud tops (≤ 240 K) for each composite (Fig. 8). Over the continent the developing composite has around a 5% higher coverage of cold cloud tops, though the differences are not significant. Upon crossing the coast the nondeveloping composite drops to below 50% coverage, consistent with a decrease in deep convection, while the developing composite remains convectively active. The composites are significantly different upon leaving the coast and for the 2 days after. Beyond this timeframe the developing waves are typically moving north out of the latitude bounds of the Hovmöller. This figure provides observational evidence of the differences in convection for the two composites in the days after they leave the coast, consistent with the results of Leppert et al. (2013b). The rest of the paper will now investigate the environmental factors influencing these differences in convective activity.

b. Environmental differences between favorable AEWs

The large-scale differences between the favorable mean developing and nondeveloping waves at the time of coastal passage are presented in Fig. 9. Two pronounced regions with significantly different total precipitable water (TPW) are shown to the west of the composite trough (Fig. 9a). Developing waves, therefore, have a region with significantly more moisture throughout the column to the northwest of the trough, while to the southwest the developing waves have significantly less moisture. These differences are located in a region of strong meridional moisture gradient. The north-south dipole structure of the anomalies suggests either a poleward shift of moisture in the developing composites or an equatorward shift of drier air in the

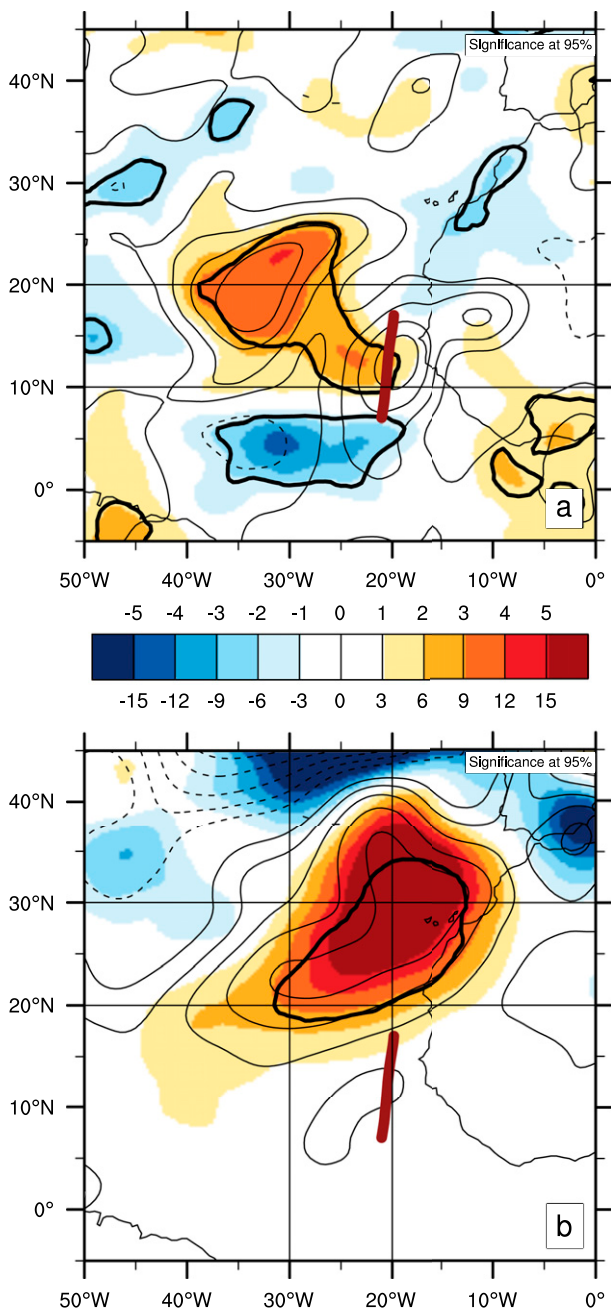


FIG. 9. Mean composite differences for favorable developing waves vs favorable nondeveloping waves (shading). Contours represent the composite favorable developing waves. The shading and contour intervals are equivalent. The color bar applies to the plot above and below with labels on the respective side of the color bar. The thick black contour encompasses the regions that are statistically significant at greater than 95%. (a) TPW (mm) and (b) 300-hPa geopotential height (gpm). Horizontal lines denote the bounds of latitudes used in Fig. 11. The vertical lines in (b) denote the cross sections shown in Fig. 10.

nondeveloping composites. The mean developing wave contours show that the increase to the northwest is a separate region of anomalously increased moisture, likely the trough of a downstream AEW trough, with a reduced ridge between the two troughs. To the south, nondeveloping waves have horizontal axes with a greater southwest–northeast tilt such that the troughs extend farther to the southwest. Since moisture is greater along the trough axis, the developing waves have less moisture in this region.

Figure 9b shows increased upper-level (300 hPa) geopotential heights representative of a weaker mid-latitude trough to the north for the developing waves. However, this upper-level feature is displaced around 1000 km north of the composite troughs. This difference is maximized at the level presented here, with significant differences extending down to around 600 hPa over the same geographical region. Associated with the differences in geopotential height are regions of significantly different wind (not shown here). Significantly increased northwesterly flow is present in the subsiding region on the western side of the midlatitude trough. The developing wave composite (contour lines) shows that the difference between developing and nondeveloping composites is comparable to the difference between the developing composite and climatology. Therefore, the nondeveloping waves have a more climatological structure with a midlatitude trough in this region. The developing waves, however, exhibit a weakened mid-latitude trough and an associated region of increased upper-level temperature anomalies.

Vertical cross sections along 30° and 20°W (depicted in Fig. 9b) showing the differences in moisture and geopotential height are presented in Fig. 10. Ahead of the trough (30°W; Fig. 10a) the differences in moisture are concentrated in the lower midtroposphere with the maxima at 850 hPa whereas the midlatitude trough at this longitude has only a small area of significant difference. While the moist anomaly around 20°N is concentrated at low levels, along 5°N the region of decreased moisture extends from the boundary layer up to 400 hPa. Along the approximate longitude of the composite trough (20°W; Fig. 10b) there are effectively no significant differences in moisture. Around 30°N, however, the developing waves exhibit increased heights with significant differences extending from 600 hPa up to around 200 hPa.

These figures reveal large regions of significantly different environmental conditions between developing and nondeveloping waves. Low-level moisture ahead of the waves is hypothesized to have a thermodynamical impact on the convection in the developing trough through entrainment into and below the midlevel vortex

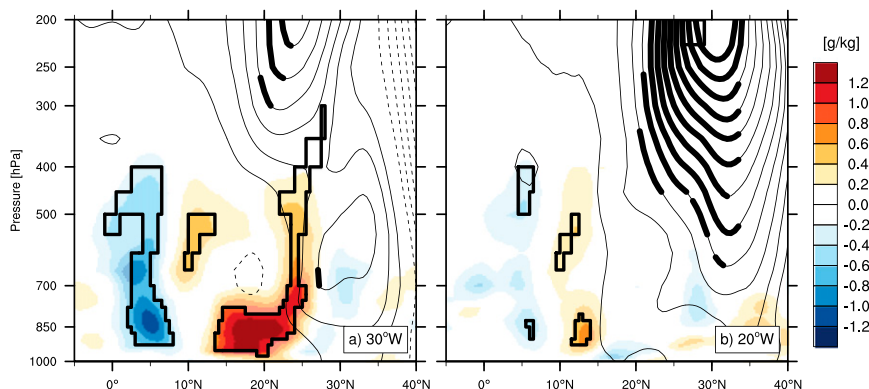


FIG. 10. Latitude–height cross section showing favorable developing waves vs favorable nondeveloping waves along (a) 30° and (b) 20°W of specific humidity (g kg^{-1}) (shading) and geopotential height every 2.5 m (contours). Bold contours and shading (outlined) denote areas of statistical significance.

of the trough. The upper-level flow north of the AEW, however, may have a less direct impact. While there are differences in the deep layer shear and upper-level temperature associated with the change in midlatitude flow, these are both restricted to north of 20°N. It is hypothesized that the presence of a trough in this region, for the nondeveloping waves, will increase subsiding equatorward flow over the eastern Atlantic and may influence the environmental humidity ahead of the AEW trough.

The time–longitude evolution of these differences is presented in Fig. 11. The latitude bands used in the Hovmöllers vary for each panel and are situated around the maximum differences in Fig. 9. The difference in moisture between the composite waves propagates westward west of the composite trough, with significant differences extending back 120 h when the troughs were over land (Fig. 11a). This difference in moisture is ahead (west) of the composited troughs over West Africa and the eastern Atlantic. Analysis of lagged maps reveals that this represents a downstream AEW trough for the developing waves, which has brought moisture anomalously far north on its eastern edge. Although this difference in moisture is present over West Africa based on the logistic regression output it appears to not influence the structure of the waves prior to the coastal region. Analysis of this northwest region could, however, provide earlier information in determining the outcome of the waves after they leave the coast.

The geopotential height differences north of the composite troughs (between 20° and 30°N) is mostly a stationary feature across the latitude bands used (Fig. 11b). Significant differences appear in both fields at around 4 days prior to the trough passage at the coast. Analysis of the total fields at these times reveals that a

more zonal flow is present in the developing composite, while the nondeveloping composite features a weak positively tilted midlatitude trough and associated meridional flow. The influence the midlatitude trough has on the eastern Atlantic is, therefore, present for around 4 days before the composited AEW troughs reach the coast. Section 5 will investigate the flow around the favorable troughs in further detail.

This subsection has highlighted the large-scale environmental differences between favorable developing and favorable nondeveloping waves. The physical mechanisms for how these differences impact the evolution of the troughs will now be explored. Analysis of the relative flow through and around the troughs throughout this time will be used to explore whether and how these environmental differences are physically linked to the changes in convection and, thus, the outcome of the favorable wave composites.

c. Relative flow through favorable AEWs

Wave-relative streamlines at two levels in the lower troposphere (850 and 700 hPa) for nondeveloping and developing waves are shown in Fig. 12. The wave relative flow is calculated by subtracting the phase speed of each wave from the wind components prior to compositing. When the troughs are over Africa, three days prior to reaching the coast (Figs. 12a,b), both composites exhibit almost zonal westerly relative flow below the AEJ (blue streamlines; 850 hPa). This is due in part to the monsoonal inflow that has a slight westerly component over this region in addition to the westward phase speed of the waves. At the jet level (red streamlines; 700 hPa), the circulation associated with the composite trough is more evident; however, a region of recirculation is not evident in the streamline analysis at this time.

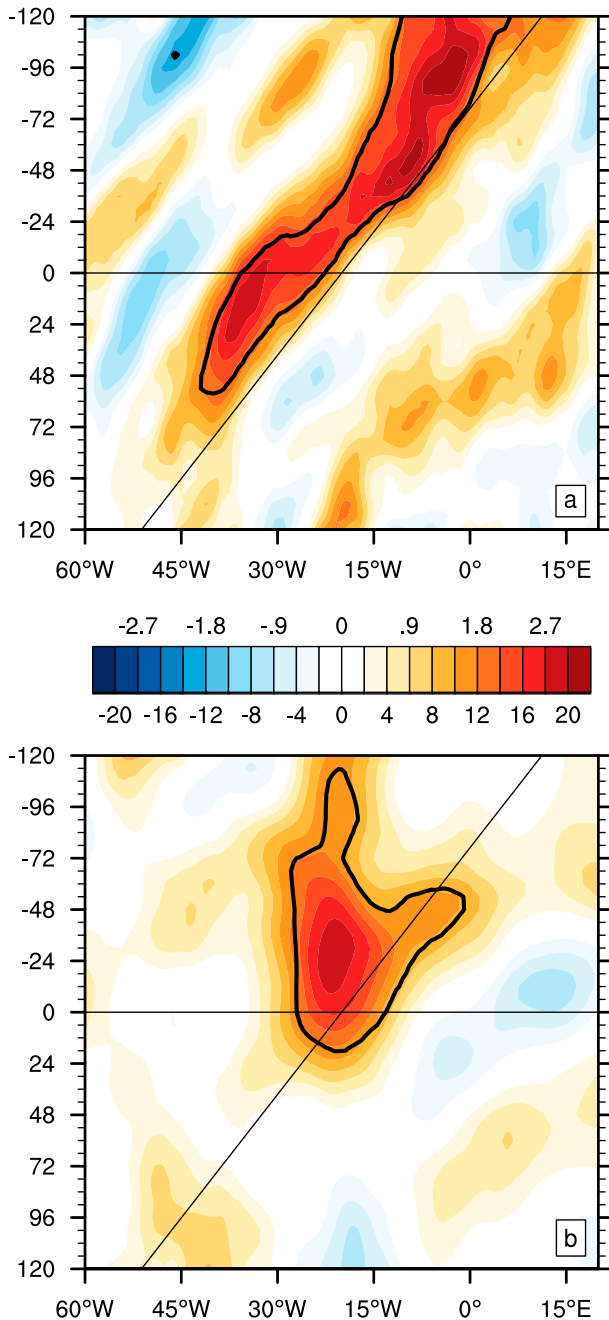


FIG. 11. Mean composite differences for favorable developing waves vs favorable nondeveloping waves for -120 to $+120$ h of leaving the African continent. Day 0 is represented with a horizontal black line. The mean track of the composite trough is depicted with a diagonal black line. Black contours encompass regions that are statistically significant greater than 95%. The color bar represents the plot above and below with labels on the respective side of the color bar. Latitude bands for each Hovmöller vary, these are shown in Fig. 9. (a) TPW (10° – 20° N; mm), (b) 300-hPa geopotential height (20° – 30° N; gpm).

By the time the waves have left the coast (Figs. 12c,d), a closed circulation has become apparent at the level of the jet. Both waves exhibit recirculation in the streamlines where the vortex is strongest and the meridional shear of the jet allows for a moderate vortex on the southern gradient of the jet to recirculate. The relative inflow below the jet (850 hPa) has changed from westerly to northwesterly. Therefore, while at the jet level air is recirculating in a 2D sense, the ascent through the layer is being sourced from outside of the trough region. Over the eastern Atlantic, 72 h after leaving the coast, both composites (Figs. 12e,f) have developed low-level recirculation regions. The nondeveloping waves are much weaker at this time, but in a quiescent background flow still have closed circulation at low levels.

From this analysis it is clear that as waves leave the coastal region, the wave-relative streamlines below the jet are temporarily open to environmental air from the north and northwest of the trough. The streamlines suggest that the air that flows under the midlevel trough appears to have an origin from north and northwest of the trough. This region had significant differences in low-level moisture between the two composites, with developing waves having significantly increased moisture to the northwest in the lower troposphere. We hypothesize that waves are sensitive to the environment northwest of the trough in the few days after crossing the West African coast. The relative advection of either moist or dry air into the lower levels of the vortex would likely influence deep convection, either helping or hindering the development process of favorable waves. As streamlines are an Eulerian view of the flow at a specific time and not representative of the time-evolving flow, the following section will present a trajectory analysis of all the waves in both subsets. The trajectories will test whether the air from the northwest quadrant is able to enter the system and also where that air originated from, providing a more complete and accurate view of the flow around favorable AEWs.

5. Trajectory analysis of developing and nondeveloping waves

The composite analysis presented in section 4 highlights some large-scale differences between two composites of waves diagnosed to be favorable for development upon leaving the coast of West Africa. Streamline analysis showed a potential kinematic route for the lower-tropospheric moisture difference to directly impact the fate of the troughs. This section will present a trajectory analysis of the relative flow in a Lagrangian frame for all favorable waves. Trajectories were analyzed with respect to each trough's track, with

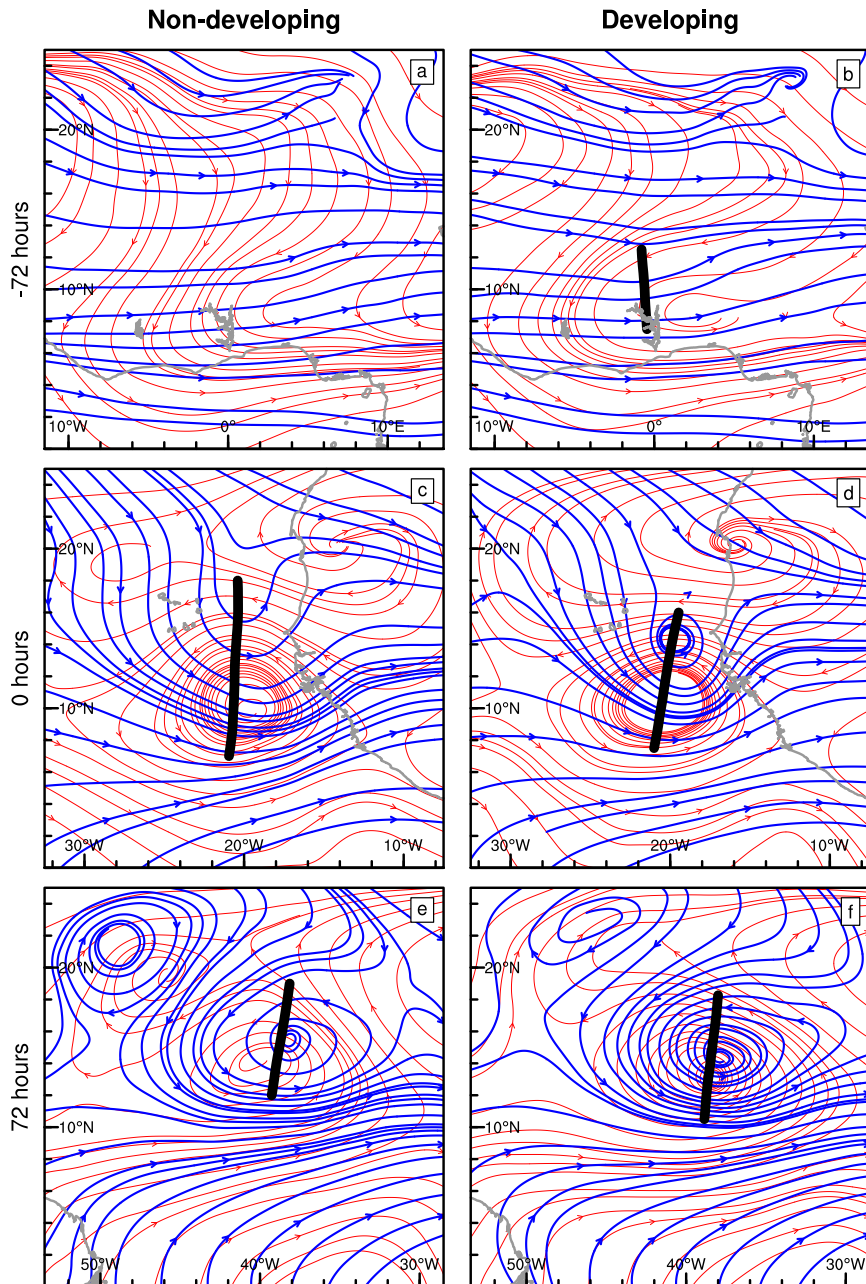


FIG. 12. Composite wave relative streamlines at two levels for (a),(b) day -3 ; (c),(d) day 0; and (e),(f) day $+3$ and favorable (left) nondeveloping and (right) developing waves. Streamlines represent 700-hPa (red) and 850-hPa (blue) wave-relative flow. Thick black contour shows the 700-hPa trough line.

those that came within 200 km of the vortex center classified as having been ingested by the system.

a. Inflow for developing and nondeveloping waves

The fraction of all trajectories from the northwest quadrant that were ingested by the system within 48 h after the trough had left the coast is shown in Fig. 13.

Consistent with the streamline analysis of the previous section, there is inflow from the northwest quadrant with around 10%–25% of the trajectories being ingested. The nondeveloping waves (Fig. 13a) have a higher fraction of ingested trajectories at greater initial distances from the trough. The developing waves (Fig. 13b) have the highest fraction of ingested

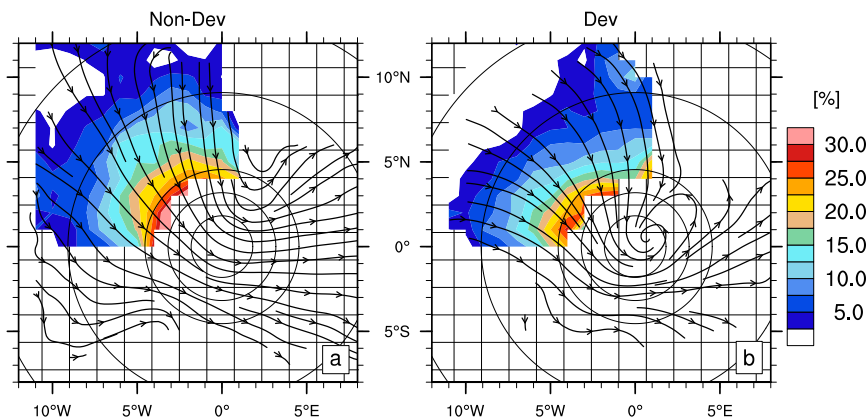


FIG. 13. Fraction of trajectories that are ingested (come within 200 km of the vortex center) by the trough. Percentage is relative to the total number of trajectories initialized at each relative grid point. Location is relative to trough center at the time of initialization. Range rings denote 200, 350, 500, 1000, and 1500 km. Streamlines depict the 48-h mean wave-relative velocity of all ingested trajectories per grid point. The hatched background covers regions in which either no trajectories were initialized or were not included in the analysis because of their initial proximity to the vortex center.

trajectories originating from west-northwest of the trough and closer than 500 km at the initial time. The streamlines represent the 48-h mean flow of the trajectories ingested by the troughs. The nondeveloping waves have westerly flow across the vortex, whereas the developing waves exhibit recirculation. As the trough strengthens, the associated cyclonic flow will become more dominant than the background environmental flow enabling the stronger vortices to develop recirculation earlier than weaker vortices. The differences between the streamlines in Fig. 13 suggest that the developing waves are experiencing this strengthening and, hence, are not as open to the environment at greater radial distances.

The northwest quadrant was targeted due to the significant differences in moisture shown in section 4. Figure 14 shows the distribution of relative humidity and pressure for the ingested trajectories at 6-h intervals relative to the time of each trajectory's closest pass to the trough center. The trajectories for the nondeveloping waves have significantly lower humidity at all time periods, though the distribution does shift toward higher humidities over time. The pressure of the trajectories is also significantly different over the first 18 h. Around 50% of trajectories ingested by the nondeveloping waves are being initialized higher than approximately 75% of those ingested by developing waves. This suggests that as the developing waves strengthen, the layer of relative inflow is reduced to lower levels. The nondeveloping waves, however, stay open to the environment over a greater depth due to the lack of strengthening.

b. Sources of environmental air for the northwest quadrant

The forward trajectories have highlighted that there is inflow into the AEWs from the northwest quadrant in the 48 h after leaving the West African coast. Backward trajectory calculations of the ingested trajectories have identified the environmental source regions for the northwest quadrant of the AEW troughs. Figure 15 shows the mean 96-h flow of the trajectories visualized by streamlines. The velocities of all trajectories were averaged to a 1° grid such that the streamlines represent the composite 96-h kinematic flow of air into the northwest quadrant of AEWs at the time the waves are just west of the West African coast. For both composites there appears to be three main sources of air into the northwest quadrant; low-level cross-equatorial flow from the south, mid- to low-level flow along the West African coast from the north, and subsiding flow along the AEJ from the east.

The sources of trajectories (96 h before reaching the northwest quadrant of the AEW trough) are split up into the three regions depicted in Fig. 15a. The frequency with respect to relative humidity and pressure is shown in Fig. 16. The trajectories from the north (Figs. 16a,b) are dominated by flow through the lower troposphere with very low humidity. Carlson and Prospero (1972) noted that air flowing along this route was generally dust free. It should be noted that for the nondeveloping cases, there are more trajectories from the northwest between 700 and 600 hPa with relative humidity values of 20%–30%. These trajectories

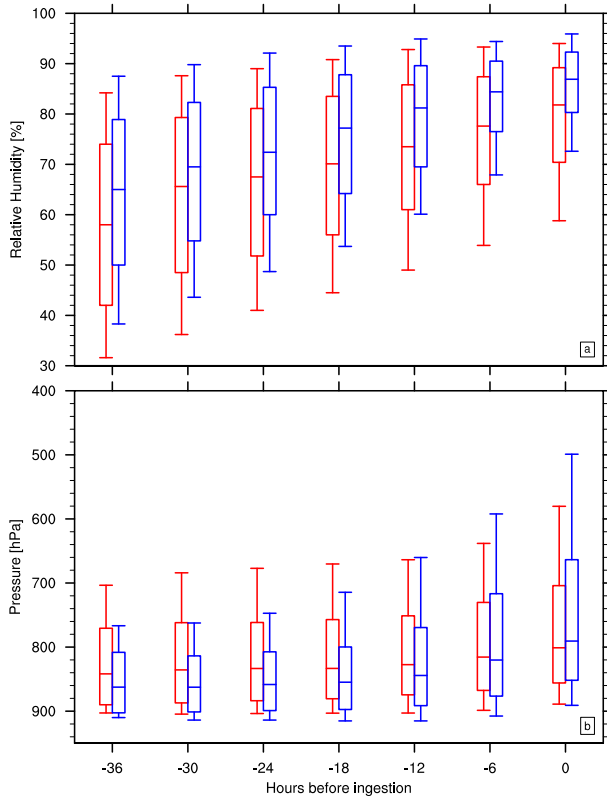


FIG. 14. Distribution of ingested (within 200 km of the vortex center) trajectory characteristics at 6-h intervals relative to the time of ingestion for nondeveloping (red) and developing (blue) waves. (a) Relative humidity of trajectories (%). (b) Pressure of trajectories (hPa).

generally subside as they approach the environment ahead of the AEW trough as shown in Fig. 15a. This flow may be enhanced in the nondeveloping cases due to the presence of a stronger midlatitude trough (see Fig. 9b). The northern box contains a higher fraction of trajectories for the nondeveloping waves compared to

the developing waves suggesting that variations in the amount of relatively dry higher-latitude air reaching the AEW environment is an important consideration. Both waves have a similar fraction of trajectories originating from the eastern box (Figs. 16c,d). These trajectories originate from around the level of the AEJ with relatively moist air with relative humidities of 60%–80%. Both subsets do exhibit lower-troposphere trajectories to the north of the AEJ, likely associated with drier Saharan air. Trajectories from this Saharan origin were analyzed separately and no significant differences between subsets were found. For the waves analyzed here, dry trajectories specifically with Saharan origin only accounted for around 5%. From the south (Figs. 16e,f) the cross-equatorial flow is confined to very low levels and is representative of a moist oceanic boundary layer air. Developing waves have around 6% more trajectories from this region compared to the nondeveloping waves, providing an increased transport of warm moist air into the northwest quadrant ahead of the troughs.

The trajectory analysis has shown that both developing and nondeveloping waves have similar kinematic flow after leaving the West African coast. Both sets of waves show a pathway for inflow from the northwest quadrant of the trough. We hypothesize, therefore, that differences in moisture ahead of the favorable waves can have a direct impact on the fate of the trough’s evolution through relative advection into the trough center at low levels. To understand why there were such differences in the moisture ahead of the troughs, back trajectories were calculated. These revealed two main differences between the subsets. Developing waves had a higher fraction of cross-equatorial flow of high humidity air. Nondeveloping waves, however, had an increase in the fraction of trajectories from the northwest with low humidity air.

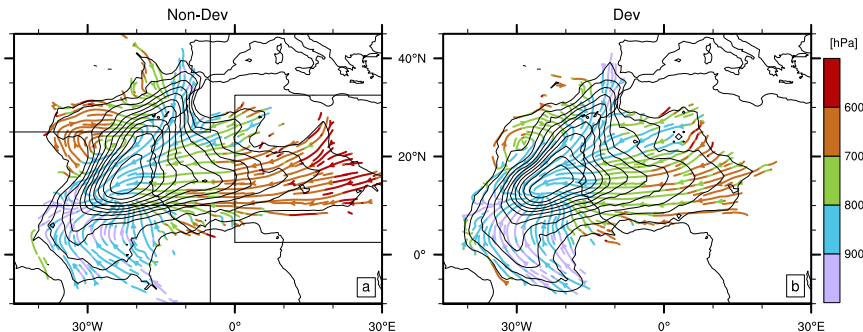


FIG. 15. Streamlines depicting the mean velocity of trajectories per 1° grid over the 96 h of backward trajectories. The color of the streamlines represents the mean pressure of the trajectories at each grid point. The contours show the log density of the trajectories. (a) Nondeveloping waves; boxes represent the three regions discussed in the text. (b) Developing waves.

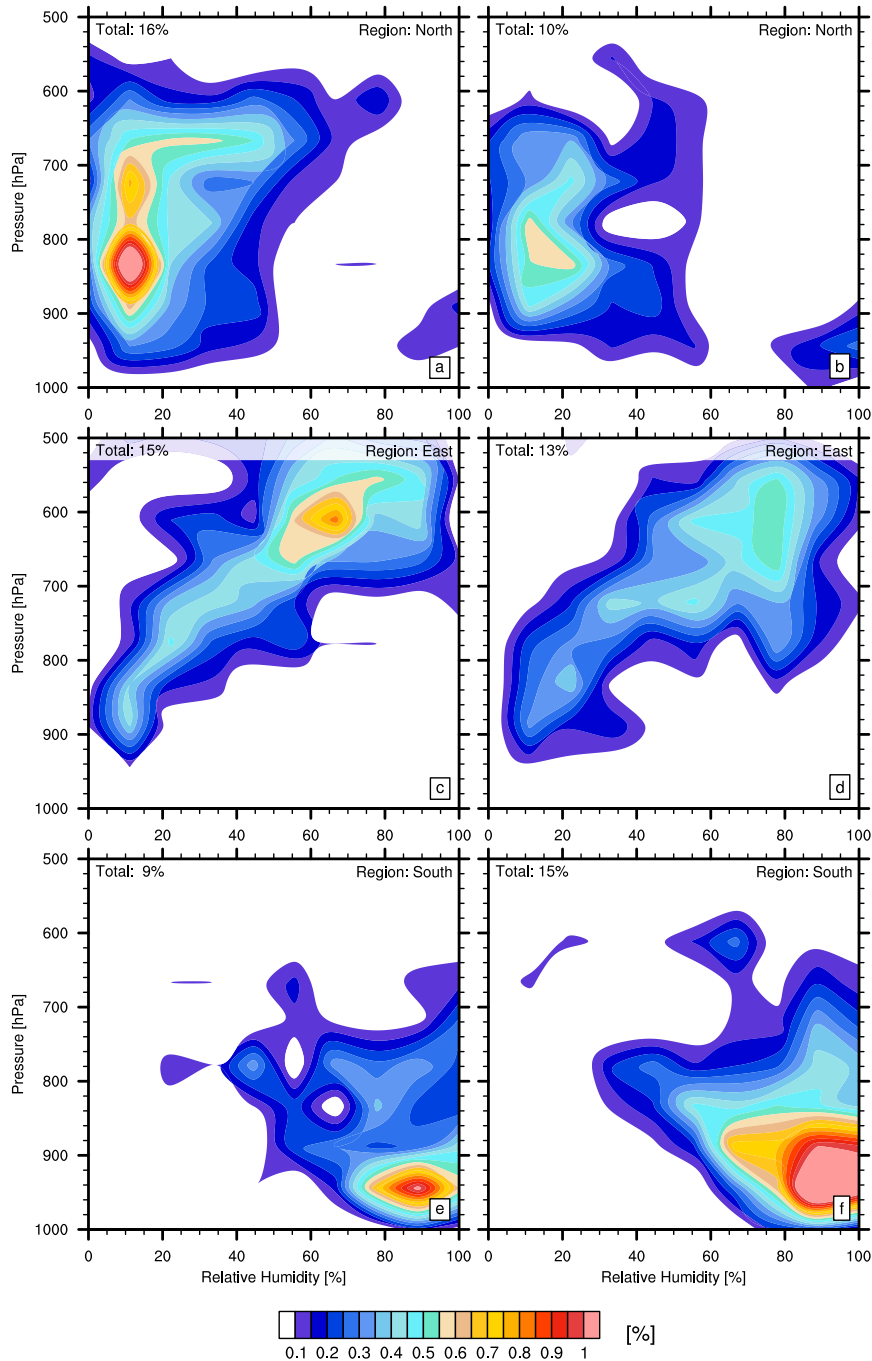


FIG. 16. Density of characteristics of the backward trajectories at -96 h. Percentages are with respect to number of trajectories calculated in each subset of waves (a),(c),(e) nondeveloping ($n = 2996$) and (b),(d),(f) developing ($n = 2575$). Rows are aligned as the (a),(b) northern region; (c),(d) eastern region; and (e),(f) southern region.

6. Conclusions

The characteristics of AEWs over the West African continent have been shown to be significantly related to the probability of tropical cyclogenesis over the eastern

Atlantic. A tracking methodology was developed and a Lagrangian evolution of developing and nondeveloping waves was presented. This analysis confirmed significant differences between developing waves and nondeveloping waves consistent with previous studies (e.g.,

Hopsch et al. 2010; Agudelo et al. 2011). A logistic regression model was used to objectively define AEWs based on a combination of trough-centric variables. The model determined that a combination of upper-level divergence and temperature, midlevel ascent, low-level vorticity, and the number of days from the peak in the AEW season are able to statistically predict the outcome of eastern Atlantic genesis from AEWs with high skill.

Based on the logistic regression model, approximately 75% of nondeveloping waves are very unfavorable for genesis over the eastern Atlantic. This result highlights that comparisons between the few developing waves and all nondeveloping waves are limited in their usefulness. The logistic regression model objectively defined waves that were used in a composite analysis of 51 developing and nondeveloping favorable waves at the West African coast. This enabled further analysis of these waves and highlighted differences in the large-scale environment.

When only favorable AEW troughs were compared, differences between the troughs were no longer significantly different prior to transition over the coast of West Africa. Composite analysis highlighted that favorable developing waves are typically associated with a region of anomalously moist air northwest of the trough as they exit the West African coast. This synoptic pattern was coincident with more zonal flow through the extratropics over the subtropical eastern Atlantic and the northwest of West Africa. Favorable nondeveloping waves conversely had drier air to the north and northwest of the trough on exiting the coast, with a midlatitude trough to the northwest of West Africa more representative of climatology over the region. The difference in moisture ahead of the composited troughs propagated with the waves over the African continent for up to 4 days prior to the coastal region. This moisture anomaly appears to be associated with downstream AEW troughs, in the developing cases, transporting moisture poleward. Therefore, the downstream wave has effectively primed the environment with moisture making the region less hostile. Conversely nondeveloping waves either lack a consistent downstream wave or move into a region with stronger low-level northerly flow over the eastern Atlantic resulting in a drier environment compared to the developing cases.

Over West Africa streamline analysis showed that the troughs were typically open to the environment at the level of the AEJ and below. The relative flow at this location was, however, primarily zonal. Therefore, although the moisture anomaly is present to the northwest the impact on the troughs may be limited. As the troughs reached the coast, the streamlines suggested that at the jet level the troughs develop a region of recirculation. At

low levels, however, because of the weaker vortex and the meridional confluence of the monsoonal flow, streamlines suggested that the waves were ingesting air from the northwest quadrant. This source of inflow was coincident with the region of anomalous moisture in the composite analysis.

Trajectories were initialized in the northwest quadrant of each wave to analyze whether the region of significantly different moisture was directly impacting the waves. The trajectories showed that between 20% and 30% of the initialized trajectories between 900 and 600 hPa came within 200 km of the troughs within 48 h. Developing waves had less inflow from the northwest quadrant compared to nondeveloping waves with the inflow restricted to lower levels. This result would support the hypothesis of recirculation within the troughs, with the strengthening vortices developing a more vertically extended region of recirculation. Dry air associated with the nondeveloping waves is able to penetrate into the AEW troughs and the distribution of trajectories stayed significantly drier. If the incipient disturbance has a more canonical lower troposphere warm-core vortex, the sensitivity to the lower troposphere environmental air is expected to be reduced. As AEWs propagate westward they generally evolve toward this low-level warm core structure (Janiga and Thorncroft 2013). Therefore, this sensitivity may be restricted to a short time span after the waves leave the West African coast. This result is in general agreement with simulations of other AEW genesis cases where the impact of dry air was restricted to the early pregenesis stages (Sippel et al. 2011), although in the cases presented here genesis is prevented rather than merely delayed.

Back trajectories revealed that nondeveloping waves have an increased fraction of trajectories from the north between about 800 and 600 hPa. This dry subsiding air impacts the moisture-sensitive region ahead of the AEWs and appears to be enhanced by the midlatitude trough that typically characterizes the eastern Atlantic. Developing waves had relatively increased cross-equatorial flow, to the west of the trough associated with the downstream wave, providing a source of moisture to the northwest quadrant of the troughs. Dry air from the Sahara was not found to have any significant differences between the two subsets of troughs analyzed here. The SAL did not appear to be a consistent feature in the waves selected here and, therefore, conclusions regarding any negative or positive impact cannot be made.

In conclusion, a major motivation for this work was the need to distinguish between developing and nondeveloping waves. Previous work identified waves that looked favorable but there still remained a lot of variability. Therefore, we have focused on highlighting the

key processes that distinguish between these favorable developing and favorable nondeveloping waves. This work has highlighted the importance of the relative flow through a pregenesis AEW over the eastern Atlantic. Based on the results here, we recommend not only monitoring the characteristics of the troughs but also the lower-tropospheric environment ahead of the wave in the days around their departure from the African continent.

Acknowledgments. The authors wish to thank three anonymous reviewers for thorough and insightful comments that greatly improved this paper. This research is supported by the NASA Grant NNX10AU44G from the Hurricane and Severe Storm Sentinel (HS3) investigation. Analysis and plotting of data were conducted using the NCAR Command Language (version 6.2.1) (NCAR 2014). The CFSR data used in this study were downloaded from the Research Data Archive (RDA), which is maintained by the Computational and Information Systems Laboratory (CISL) at the National Center for Atmospheric Research (NCAR). NCAR is sponsored by the National Science Foundation (NSF). The original CFSR data are available from the RDA (<http://rda.ucar.edu>) in dataset numbers ds093.0. The daily outgoing longwave radiation data used in this research was provided by NOAA/OAR/ESRL PSD, Boulder, Colorado, from their website at http://www.esrl.noaa.gov/psd/data/gridded/data.interp_OLR.html.

REFERENCES

- Agudelo, P., C. D. Hoyos, J. Curry, and P. J. Webster, 2011: Probabilistic discrimination between large-scale environments of intensifying and decaying African easterly waves. *Climate Dyn.*, **36**, 1379–1401, doi:10.1007/s00382-010-0851-x.
- Bain, C. L., K. D. Williams, S. F. Milton, and J. T. Heming, 2014: Objective tracking of African easterly waves in Met Office models. *Quart. J. Roy. Meteor. Soc.*, **140**, 47–57, doi:10.1002/qj.2110.
- Berry, G. J., and C. D. Thorncroft, 2005: Case study of an intense African easterly wave. *Mon. Wea. Rev.*, **133**, 752–766, doi:10.1175/MWR2884.1.
- , —, and T. Hewson, 2007: African easterly waves during 2004—Analysis using objective techniques. *Mon. Wea. Rev.*, **135**, 1251–1267, doi:10.1175/MWR3343.1.
- Braun, S. A., J. A. Sippel, and D. S. Nolan, 2012: The impact of dry midlevel air on hurricane intensity in idealized simulations with no mean flow. *J. Atmos. Sci.*, **69**, 236–257, doi:10.1175/JAS-D-10-05007.1.
- Carlson, T. N., and J. M. Prospero, 1972: The large-scale movement of Saharan air outbreaks over the northern equatorial Atlantic. *J. Appl. Meteor.*, **11**, 283–297, doi:10.1175/1520-0450(1972)011<0283:TLSMOS>2.0.CO;2.
- Cecelski, S. F., and D.-L. Zhang, 2013: Genesis of Hurricane Julia (2010) within an African easterly wave: Low-level vortices and upper-level warming. *J. Atmos. Sci.*, **70**, 3799–3817, doi:10.1175/JAS-D-13-043.1.
- Chen, T.-C., S.-Y. Wang, and A. J. Clark, 2008: North Atlantic hurricanes contributed by African easterly waves north and south of the African easterly jet. *J. Climate*, **21**, 6767–6776, doi:10.1175/2008JCLI2523.1.
- DeMaria, M., and J. Kaplan, 1994: A Statistical Hurricane Intensity Prediction Scheme (SHIPS) for the Atlantic basin. *Wea. Forecasting*, **9**, 209–220, doi:10.1175/1520-0434(1994)009<0209:ASHIPS>2.0.CO;2.
- Draxler, R. R., and G. D. Hess, 1998: An overview of the HYSPLIT_4 modelling system for trajectories, dispersion, and deposition. *Aust. Meteor. Mag.*, **47**, 295–308.
- Dunion, J. P., and C. S. Velden, 2004: The impact of the Saharan air layer on Atlantic tropical cyclone activity. *Bull. Amer. Meteor. Soc.*, **85**, 353–365, doi:10.1175/BAMS-85-3-353.
- , J. Kaplan, A. Schumacher, J. Cossuth, and M. DeMaria, 2013: Development of a Probabilistic Tropical Cyclone Genesis Prediction Scheme. JHT Year 2 End of Year Report. Tech. Rep., 4 pp. [Available online at http://www.nhc.noaa.gov/jht/11-13reports/Final_Dunion_JHT13.pdf.]
- Dunkerton, T., M. Montgomery, and Z. Wang, 2009: Tropical cyclogenesis in a tropical wave critical layer: Easterly waves. *Atmos. Chem. Phys.*, **9**, 5587–5646, doi:10.5194/acp-9-5587-2009.
- Emanuel, K. A., 1989: The finite-amplitude nature of tropical cyclogenesis. *J. Atmos. Sci.*, **46**, 3431–3456, doi:10.1175/1520-0469(1989)046<3431:TFANOT>2.0.CO;2.
- Fritz, C., and Z. Wang, 2013: A numerical study of the impacts of dry air on tropical cyclone formation: A development case and a nondevelopment case. *J. Atmos. Sci.*, **70**, 91–111, doi:10.1175/JAS-D-12-018.1.
- Ge, X., T. Li, and M. Peng, 2013: Effects of vertical shears and midlevel dry air on tropical cyclone developments. *J. Atmos. Sci.*, **70**, 3859–3875, doi:10.1175/JAS-D-13-066.1.
- Gray, W., 1968: Global view of the origin of tropical disturbances and storms. *Mon. Wea. Rev.*, **96**, 669–700, doi:10.1175/1520-0493(1968)096<0669:GVOTOO>2.0.CO;2.
- Hodges, K., B. J. Hoskins, J. Boyle, and C. D. Thorncroft, 2003: A comparison of recent reanalysis datasets using objective feature tracking: Storm tracks and tropical easterly waves. *Mon. Wea. Rev.*, **131**, 2012–2037, doi:10.1175/1520-0493(2003)131<2012:ACORRD>2.0.CO;2.
- Hopsch, S. B., C. D. Thorncroft, and K. R. Tyle, 2010: Analysis of African easterly wave structures and their role in influencing tropical cyclogenesis. *Mon. Wea. Rev.*, **138**, 1399–1419, doi:10.1175/2009MWR2760.1.
- Janiga, M. A., and C. D. Thorncroft, 2013: Regional differences in the kinematic and thermodynamic structure of African easterly waves. *Quart. J. Roy. Meteor. Soc.*, **139**, 1598–1614, doi:10.1002/qj.2047.
- Kiladis, G. N., C. D. Thorncroft, and N. M. J. Hall, 2006: Three-dimensional structure and dynamics of African easterly waves. Part I: Observations. *J. Atmos. Sci.*, **63**, 2212–2230, doi:10.1175/JAS3741.1.
- Laken, B. A., H. Parviainen, E. Pallé, and T. Shahbaz, 2014: Saharan mineral dust outbreaks observed over the North Atlantic island of La Palma in summertime between 1984 and 2012. *Quart. J. Roy. Meteor. Soc.*, **140**, 1058–1068, doi:10.1002/qj.2170.
- Landsea, C. W., 1993: A climatology of intense (or major) Atlantic hurricanes. *Mon. Wea. Rev.*, **121**, 1703–1713, doi:10.1175/1520-0493(1993)121<1703:ACOIMA>2.0.CO;2.
- , A. Hagen, W. Bredemeyer, C. Carrasco, D. A. Glenn, A. Santiago, D. Strahan-Sakoskie, and M. Dickinson, 2014: A reanalysis of the 1931–43 Atlantic hurricane database. *J. Climate*, **27**, 6093–6118, doi:10.1175/JCLI-D-13-00503.1.

- Leppert, K. D., II, D. J. Cecil, and W. A. Petersen, 2013a: Relation between tropical easterly waves, convection, and tropical cyclogenesis: A Lagrangian perspective. *Mon. Wea. Rev.*, **141**, 2649–2668, doi:10.1175/MWR-D-12-00217.1.
- , W. A. Petersen, and D. J. Cecil, 2013b: Electrically active convection in tropical easterly waves and implications for tropical cyclogenesis in the Atlantic and East Pacific. *Mon. Wea. Rev.*, **141**, 542–556, doi:10.1175/MWR-D-12-00174.1.
- Liebmann, B., and C. Smith, 1996: Description of a complete (interpolated) outgoing longwave radiation dataset. *Bull. Amer. Meteor. Soc.*, **77**, 1275–1277.
- Ling, J., and C. Zhang, 2013: Diabatic heating profiles in recent global reanalyses. *J. Climate*, **26**, 3307–3325, doi:10.1175/JCLI-D-12-00384.1.
- Martin, E. R., and C. D. Thorncroft, 2014: The impact of the AMO on the West African monsoon annual cycle. *Quart. J. Roy. Meteor. Soc.*, **140**, 31–46, doi:10.1002/qj.2107.
- Matthews, A. J., and G. N. Kiladis, 1999: The tropical–extratropical interaction between high-frequency transients and the Madden–Julian oscillation. *Mon. Wea. Rev.*, **127**, 661–677, doi:10.1175/1520-0493(1999)127<0661:TTEIBH>2.0.CO;2.
- NCAR, 2014: The NCAR Command Language (version 6.2.1). UCAR/NCAR/CISL/TDD, Boulder, CO, accessed 4 September 2014, doi:10.5065/D6WD3XH5.
- Neumann, C. J., M. B. Lawrence, and E. L. Caso, 1977: Monte Carlo significance testing as applied to statistical tropical cyclone prediction models. *J. Appl. Meteor.*, **16**, 1165–1174, doi:10.1175/1520-0450(1977)016<1165:MCSTAA>2.0.CO;2.
- Reed, R. J., D. C. Norquist, and E. E. Recker, 1977: The structure and properties of African wave disturbances as observed during phase III of GATE. *Mon. Wea. Rev.*, **105**, 317–333, doi:10.1175/1520-0493(1977)105<0317:TSAPOA>2.0.CO;2.
- Saha, S., and Coauthors, 2010: The NCEP Climate Forecast System Reanalysis. *Bull. Amer. Meteor. Soc.*, **91**, 1015–1057, doi:10.1175/2010BAMS3001.1.
- Schenkel, B. A., and R. E. Hart, 2012: An examination of tropical cyclone position, intensity, and intensity life cycle within atmospheric reanalysis datasets. *J. Climate*, **25**, 3453–3475, doi:10.1175/2011JCLI4208.1.
- Schreck, C. J., III, L. Shi, J. P. Kossin, and J. J. Bates, 2013: Identifying the MJO, equatorial waves, and their impacts using 32 years of HIRS upper-tropospheric water vapor. *J. Climate*, **26**, 1418–1431, doi:10.1175/JCLI-D-12-00034.1.
- Schumacher, C., R. A. Houze Jr., and I. Kraucunas, 2004: The tropical dynamical response to latent heating estimates derived from the TRMM Precipitation Radar. *J. Atmos. Sci.*, **61**, 1341–1358, doi:10.1175/1520-0469(2004)061<1341:TDRTL>2.0.CO;2.
- Shu, S., and L. Wu, 2009: Analysis of the influence of Saharan air layer on tropical cyclone intensity using AIRS/Aqua data. *Geophys. Res. Lett.*, **36**, L09809, doi:10.1029/2009GL037634.
- Sippel, J. A., S. A. Braun, and C.-L. Shie, 2011: Environmental influences on the strength of Tropical Storm Debby (2006). *J. Atmos. Sci.*, **68**, 2557–2581, doi:10.1175/2011JAS3648.1.
- Stanski, H. R., L. J. Wilson, and W. R. Burrows, 1989: Survey of common verification methods in meteorology. World Weather Watch Tech. Rep. 8, WMO/TD 358, World Meteorological Organization, 81 pp.
- Stohl, A., G. Wotawa, P. Seibert, and H. Kromp-Kolb, 1995: Interpolation errors in wind fields as a function of spatial and temporal resolution and their impact on different types of kinematic trajectories. *J. Appl. Meteor.*, **34**, 2149–2165, doi:10.1175/1520-0450(1995)034<2149:IEIWFA>2.0.CO;2.
- Thorncroft, C. D., and K. Hodges, 2001: African easterly wave variability and its relationship to Atlantic tropical cyclone activity. *J. Climate*, **14**, 1166–1179, doi:10.1175/1520-0442(2001)014<1166:AEWVAI>2.0.CO;2.
- , and I. Pytharoulis, 2001: A dynamical approach to seasonal prediction of Atlantic tropical cyclone activity. *Wea. Forecasting*, **16**, 725–734, doi:10.1175/1520-0434(2002)016<0725:ADATSP>2.0.CO;2.
- Wang, Z., M. T. Montgomery, and T. Dunkerton, 2010: Genesis of pre-Hurricane Felix (2007). Part I: The role of the easterly wave critical layer. *J. Atmos. Sci.*, **67**, 1711–1729, doi:10.1175/2009JAS3420.1.
- Wilks, D. S., 2011: *Statistical Methods in the Atmospheric Sciences*. 3rd ed. Academic Press, 704 pp.
- Zhang, C., and S. M. Hagos, 2009: Bimodal structure and variability of large-scale diabatic heating in the tropics. *J. Atmos. Sci.*, **66**, 3621–3640, doi:10.1175/2009JAS3089.1.